공학석사 학위논문

산화철을 함유한 히알루론산 나노입자를 이용한 페롭토시스 암세포사멸 조절에 관한 연구

Study on regulation of ferroptotic cancer cell death using iron oxide-containing hyaluronic acid nanoparticles

2019 년 2 월

서울대학교 대학원

융합과학부 나노융합전공

배 채 원

산화철을 함유한 히알루론산 나노입자를 이용한 페롭토시스 암세포사멸 조절에 관한 연구

Study on regulation of ferroptotic cancer cell death using iron oxide-containing hyaluronic acid nanoparticles

지도 교수 이 강 원

이 논문을 공학석사 학위논문으로 제출함

2019 년 1 월

서울대학교 대학원

융합과학부 나노융합전공

배 채 원

배 채 원의 공학석사 학위논문을 인준함

2019 년 1 월

위 원 장 _____ (인)

부위원장 _____ (인)

위 원 _____ (인)

Abstract

Study on regulation of ferroptotic cancer cell death using iron oxide-containing hyaluronic acid nanoparticles

Chaewon Bae

Program in Nano Science and Technology

Graduate School of Convergence Science and Technology

Seoul National University

Ferroptosis is a recently recognized form of regulated cell death by iron-dependent reactive oxygen species (ROS) and lipid peroxidation that different from traditional apoptosis and necrosis. Iron (Fe), an essential transition metal ion for life, plays a vital role in regulating cell death. Here, we fabricated cancer-targeting nanoparticles (NPs) by fine-tuning physicochemical properties to regulate the lysosomal activity via cellular iron equilibria and ROS generation. We observed iron-dependent cell death by analyzing cellular uptake and cytotoxicity using cancer-targeting NPs

including iron. From these results, we believe that this newly proposed platform to inhibit tumor growth by regulating ROS expression and lipid peroxidation is a promising system in therapeutic applications. Together with the facile synthesis technique and obvious effect, this new iron-hyaluronic acid NPs platform is expected to be one of the effective tools for cancer therapy.

Keyword: Ferroptosis, Cancer nanomedicine, Iron-based nanoparticles, Fenton reaction, Reactive oxygen species

Student Number : 2017-25383

Table of Contents

List of Figures

Chapter 1. Introduction

Cancer nanomedicine has constantly been advanced in the therapeutic field, providing new hope and opportunities as cancer therapy to overcome complexity and heterogeneity of cancer.[1−4] There are various kinds of nanotherapy, recent research has been applied nanoparticles (NPs) that can reduce the side effect and make precise targeting are actively progressing. Hence, particle size, shape, and composition are critical to nanomedicine and must be carefully designed in nanoparticle−based therapies.[5−7] Many groups have been studying to overcome heterogeneous tumor properties and to target cells using optimal materials and components, but there are still many problems including toxicity, biocompatibility, and biodegradability.[8, 9]

Cancer nanomedicine using NPs has been studied based on apoptosis, necrosis and necroptosis and their mechanism.[10−13] For a long time, the interrelationships of iron (Fe) and cancer have not been clearly elucidated by accurate theory. In 2012, ferroptosis has been proposed that induced cell death by Fe.[14, 15] Fe is an essential transition metal in our body that plays an important role in mitochondria to produce reactive oxygen species(ROS) as well as ATP synthesis, induce lipid peroxidation of saturated fatty acids

and regulate cell death.[16] Although the mechanism for ferroptosis has not been completely elucidated, recent studies have proposed potential of ferroptosis that will be a new alternative to cancer nanomedicine.[17, 18]

Herein, we focused on cancer-targeting NPs by ferroptosis that regulate the ferroptotic activity via cellular Fe equilibria and ROS generation by fine-tuning their physicochemical properties to target cancer cells. We have developed a biocompatible and biodegradable NP platform with essential components of our body, hyaluronic acid (HA) NP, including Fe (FHA NPs), which induce ferroptosis. The newly proposed NP platform is expected to be a new alternative to the new cancer nanomedicine by overcoming the material limitations without toxicity and side effects and working effectively throughout the system to cancer therapy.

Chapter 2. Experiment

2.1 Preparation of iron/hyaluronic acid nanoparticles (FHA NPs)

Sodium hyaluronate (5 mg) was dissolved in 50 mL of deionized water (DW) and kept stirring until the HA dissolved completely. $FeCl_2 \cdot 4H2O$ (99.4 mg) in DW (10 mL) was slowly added into HA aqueous solution at a rate of 1mL per minute with stirring for 30 minutes. After then, $FeCl_3 \cdot 6H_2O$ (149.1 mg) in DW (10 mL) was slowly added to this solution by the same rate. After 1 hour under stirring, ammonia solution (1.5 M in DW) was added to adjust the pH of the solution to pH 10 as the co-precipitation method. Followed by stirring for 30 minutes, the product was separated from the solution using a strong magnet, washed with DW several times, and then re-dispersed in 50 mL of 0.005 M HCl by bath sonication. The NPs homogeneously and sufficiently dispersed were further purified by dialysis (MW cutoff 3.5K) for 24 hours and stored at −4 ℃.

2.2 Characterization of FHA NPs

Dynamic light scattering (DLS), polydispersity index (PDI) and ζ-potential of the NPs were measured using the zetasizer Nano ZS (Malvern Instruments, UK). UV-visible absorption spectrum of FHA NPs was analyzed using a microplate reader (Synergy H1, Hybrid reader, Bio Tek, VT, USA). The surface topography and morphology of the FHA NPs were observed using a field-emission scanning electron microscope (FE-SEM) (JSM-7800F Prime, JEOL Ltd., Japan) and Energy-Filtering Transmission electron microscopy (TEM) (LIBRA 120, Carl Zeiss, Germany) which was operated at an accelerating voltage of 120kV, respectively. Quantification of the amount of iron in particles was analyzed by inductively coupled plasma-atomic emission spectroscopy (ICP-AES) (Optima 8300; Perkin-Elmer, USA).

2.3 Cell culture

Human fibroblast cells (HFB), human breast adenocarcinoma cells (MCF7), human colon carcinoma cells (HCT116), human lung carcinoma cells (A549) were purchased from Koran Cell Line Bank (Seoul, Korea). HFB were maintained in Dulbecco's Modified Eagle Medium (DMEM), supplemented with 10% fatal bovine

serum(FBS) (Cellsera, NSW, Australia) and 1% penicillin/streptomycin (Welgene, Korea). All cancer cells were cultured in RPMI 1640 (Welgene, Korea), supplemented with 10% FBS and 1% penicillin/streptomycin. All cells were incubated at 37 ℃ in a humidified atmosphere of 5 % CO_2 incubator.

2.4 Cell viability

The cell viability was analyzed by WST assay using EZ-Cytox, (DoGen, Korea). All cells were plated in 96-well plate (1×10^4 cells/well) with a medium. After incubating for 24 hours, the cells were washed once with Dulbecco's phosphate buffered saline (DPBS) and FHA NPs suspensions with different concentrations (6.25, 12.5, 25, 50, 100, 200 μg/mL) in serum-free medium were treated to each well and then incubated for 1, 3, 6 and 12 hours at 37℃, respectively. After adding, 10 μL of EZ-Cytox solution in each well, cells were incubated for an additional 3 hours, and the optical density (OD) was measured at 450nm using microplate reader (Synergy H1, Hybrid reader, Bio Tek, VT, USA).

2.5 Live and Dead assay

Cells were maintained in 24 well-plates at 5×10^4 cells per well for 24hours. Different concentrations (6.25, 12.5, 25, 50, 100, 200 μg /mL) of FHA NPs in serum-free medium were treated in each well and incubated for 12hours. After washing with DPBS to remove residual FHA NPs, 2 μM Calcein AM and 4 μM Ethidium homodimer-1(EthD-1) were treated 30 minutes before fluorescence imaging at room temperature. The live cells and dead cells show green fluorescence by Calcein AM and red fluorescence by EthD-1, respectively. The live and dead cells were observed under a laser scanning microscope (Carl Zeiss, Oberkochen, Germany).

2.6 Reactive oxygen species (ROS) analysis

Detection of intracellular ROS was performed by using the CellROX Orange Oxidative Stress Reagent (Invitrogen, Carlsbad, CA, USA). Briefly, cells were plated in 24-well plates at 5×10^4 cells per well and incubated for 24 hours. Different concentrations (6.25, 12.5, 25, 50, 100, 200 μg/mL) of FHA NPs in fresh medium were treated for another additional 12 hours. After washing three times with DPBS, the CellROX Orange Oxidative Stress Reagent was

directly added to 300 μL at a final concentration of 5 μmol/L and incubated at 37℃. After 30 minutes, 4, 6-diamidino-2-phenylindole (DAPI; Sigma Aldrich, MO, USA) was added for 5 minutes to counterstain nuclei. To confirm the qualitative evaluation of intracellular ROS distribution, the labeled cells were visualized using a laser scanning microscope (Carl Zeiss, Oberkochen, Germany). For quantifying of fluorescence, each of the cells (1×10^5cells) were incubated with different concentration of FHA NPs for 12 hours, and cells detached with trypsin/EDTA. The labeled cells analyzed by Guava EasyCyte flow cytometry (Millipore, Boston, USA) and FCS Express V3 software (De Novo Software, Los Angeles, USA).

2.7 Real-time reverse transcriptase-polymerase chain reaction (real time RT-PCR)

Total RNA was isolated by trizol method (Life technologies, CA, USA), and cDNA was synthesized using cDNA synthesis kit (Maxime RT PreMix, Intron, Korea). cDNA with RealMOD Green SF 2X qPCR mix (iNtRon Biotechnology, Korea) were amplified by real time RT-PCR using QuantStudio5 Real-Time PCR system (Applied Biosystems, USA) with the following parameters: initial activation

10 minutes of denaturing at 95 ℃, followed by 40 cycles of 15s of denaturing at 95 ℃, 30secpmds of annealing at 60 ℃ and a final extension step of 5 minutes at 72 ℃. The primer sequences were used as followed; Bax were 5′ -AGGCGGCGGGCCCACCAGCTC-3′ (sense) and 5′ -CATCAGCAAACATGTCAGCTG-3′ (antisense), Ripk1 were 5′ -GGCATTGAAGAAAAATTTAGGC-3′ (sense) and 5′ -TCACAACTGCATTTTCGTTTG-3′ (antisense), GPX4 were 5′ -ACAAGAACGGCTGCGTGGTGAA-3′ (sense) and 5′ -GCCACACACTTGTGGAGCTAGA-3′ (antisense) and the primer for β-Actin were 5′ -GTGGGCCGCTCTAGGCACCAA-3′ (sense) and 5′ -CTTTAGCACGCACTGTAGTTTCTC-3′ (antisense). The quantity of mRNA was determined using the comparative $\triangle\triangle C_T$ method and normalized by the expression of β-Actin.

2.8 Prussian blue staining

For prussian blue staining, 5×10^4 cells per well were seeded to 8-well glass chamber slide (SPL Life Sciences, Korea), for 24 hours. After incubation with FHA NPs, the cells were washed with PBS three times and fixed with paraformaldehyde (4%) for 15minitues. The cells were stained with the mixture of 5 wt% prussian blue ($C_6Fe_2KN_6{\cdot}xH_2O$) (Sigma Aldrich, USA) and 10% HCl

(1:1) for 30 minutes. After washing three times with PBS, cells were counterstained using nuclear fast red (TCI, Tokyo, Japan) dissolving aluminum sulfate in DW for 5 min. After rinsing three times with PBS, the stained cells were dehydrated through 10%, 90%, and 100% alcohol, respectively, and then cleared in xylene for 3minutes. Cells were coverslipped using permanent aqueous mounting medium (Dako, USA) for microscopic study.

2.9 Inhibition assay

Cells were prepared the same condition described above in 5. Cell viability. FHA NPs were added into each well with ferrostatin-1 (Sigma Aldrich, USA), RSL3 (Selleckchem, Houston, TX, USA) and α-tocopherol (vitamin E) (Sigma Aldrich, USA), and then EZ-Cytox were performed after 12 hours.

2.10 Animal models and tumor inoculation

All animal studies were conducted in accordance with the Institutional Animal Care and Use Committee (IACUC) guidelines. Four to five-week-old male athymic Balb/c mice (17±1g) were purchased from Dooyeol Biotech, Inc. (Seoul, Korea). Mice were kept at 25±1℃ and 12/12h light/dark cycle with supplying

adequate water and food (Woojungbio., Co., LTD., Suwon, Korea). To develop the tumor model, A549 cells (2.5×10^6 cells per 100μL) were subcutaneously injected into the left and right legs of a mouse. Average initial tumor volumes of ≈330mm^3 were used for all studies. For *in vivo* studies, A549 tumor-bearing mice were divided into seven groups, and three animals per group. Then, mice were peritumoral injected with FHA NPs (8 mg/kg) every 24 hours. Control mice were injected with PBS with an equivalent volume. The tumor growth was monitored every two days by measuring perpendicular diameters with a caliper. The tumor volume was calculated with the following equation.

$$V = \frac{Width^2 \times Length}{2}$$

2.11 *Ex vivo* MRI

FHA NPs was injected every day for 14 days. Ex vivo MRI by FHA NPs accumulation was monitored in the whole tumor and normal tissues (heart, spleen, liver, kidney, and lung). MRI experiments were performed on Bruker Biospec 7T system (BioSpec 70/20 USR; Bruker, Germany) using a 35mm quadrature volume coil. The scanning parameters were TR = 200 ms, TE = 10 ms, slice thickness 1mm, average.

2.12 Histological analysis

After scarification and remove tumor from mice, tumors were fixed with 3.7% formaldehyde (Dana Korea, Korea) for 12hours and saturated with 30% sucrose in PBS. For histology, frozen tumor embedded in optimum cutting temperature (OCT) compound (Leica, USA) and stored at −80 ℃. The cryo-sections with 10 μm thickness were hematoxylin and eosin (H&E) stained. Stained tumors were then viewed under an inverted microscope (Nikon eclipse, TE2000−U, Japan).

Chapter 3. Results and Discussion

Figure 1 shows our strategy using FHA NPs as the tumor-targeted system. The interaction between HA and receptor CD44 causes receptor-mediated endocytosis leading to intracellular signaling and response.[22] After endocytosis, FHA NPs is degraded by endogenous hyaluronidase (HAase) in the lysosome, then releasing Fe, inducing ROS, and occurring cell death by lipid peroxidation, sequentially. HA containing several functional groups such as glucuronic acid, N-acetyl-glucosamine hydroxyl carboxylate is a non-immunogenic, biocompatible, biodegradable, and non-toxic polysaccharide molecule that exists in our body, therefore it has been applied to various fields such as drug delivery. To prepare the FHA NPs, we induced co-precipitation with HA, a receptor that binds to CD44 overexpressed in cancer cells, and Fe, an essential element of the body (**Figure 2a).** [19,20,21]

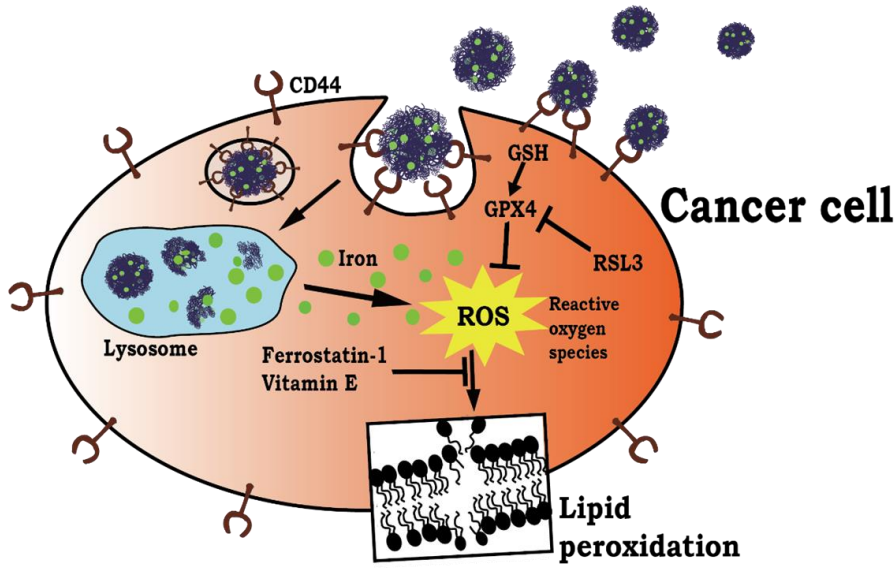

Figure 1. Schematic illustration of the overall process in which ferroptosis occurred by FHA nanoparticles.

The HA, negative charge, and Fe^{2+}/Fe^{3+}, in the FHA NPs interact with each other to form strengthened chain by secondary bonding. [23] The size distribution of FHA NPs by dynamic light scattering (DLS) was plotted (**Figure 2b**) as a function of concentration of HA at 0.005, 0.01, 0.05, 0.5 wt%. The size distribution of FHA NPs was the mean diameter of about 102±5 nm when the concentration of HA was used as the 0.01 wt%. For further studies, we used FHA NPs of 0.01 HA wt%. The X-ray diffraction (XRD) patterns were confirmed by comparing FHA NPs and HA patterns. **Figure 2c** shows a certain peak appeared like Fe oxide NPs which characteristic peaks at 2θ = 30.3 °, 35.8 °, 43.5 °, 53.9 °, and 57.3 ° 62.8° were indexed to (220), (311), (400), (422), (511), and (440), respectively. These result showed that the NPs are Fe_3O_4 with a reversed cubic spinal structure. That was confirmed that FHA NPs was carried in the iron oxide form of Fe_3O_4 among the HA polymer through co-precipitation. [24]

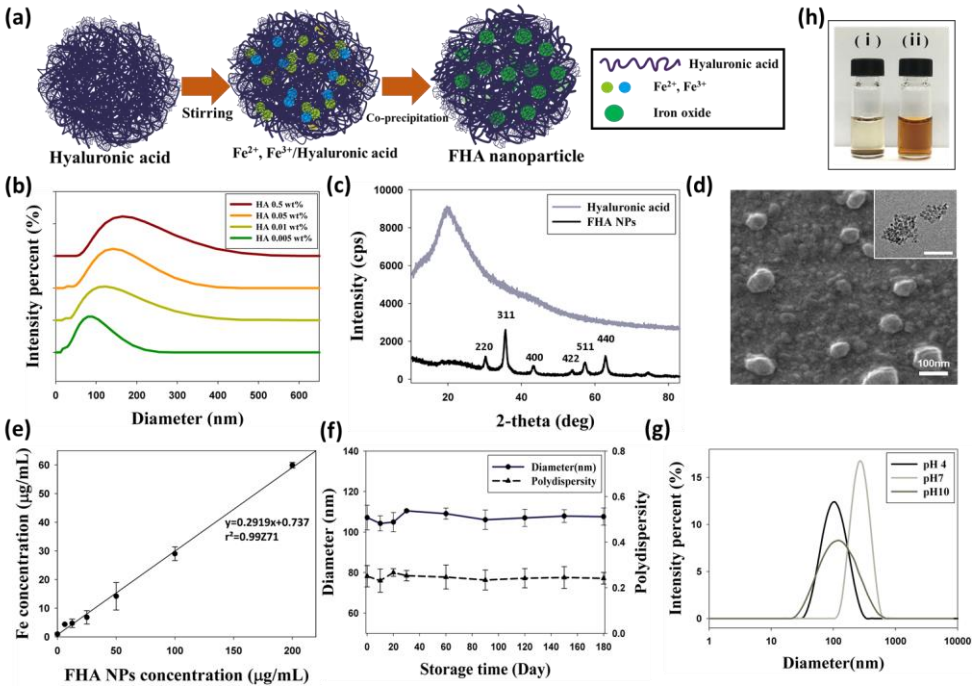

Figure 2. Characterization and Stability study of FHA nanoparticles (a) Schematic diagram for the synthesis of FHA nanoparticles. (b) Size distribution of FHA NPs against 0.005, 0.01, 0.05 and 0.5 wt% HA. (c) X-ray Diffraction Patterns of FHA Nanoparticles and HA Polymers. (d) SEM and TEM images of FHA nanoparticles. Scale bar: 100nm (e) Quantification of internalized nanoparticles by ICP-AES. (f) Stability of FHA NPs, where the size and polydispersity index (PDI) were maintained for 6 months. The graph presents the change of particle size and PDI in the storage condition. (g) DLS particle size distribution profiles confirmed at conditions of pH 4, 7, and 10 in aqueous solutions. (h) Photo image for confirming the

difference between the state stored in DW(ⅰ) and the particle stored in 0.005M HCl(ⅱ).

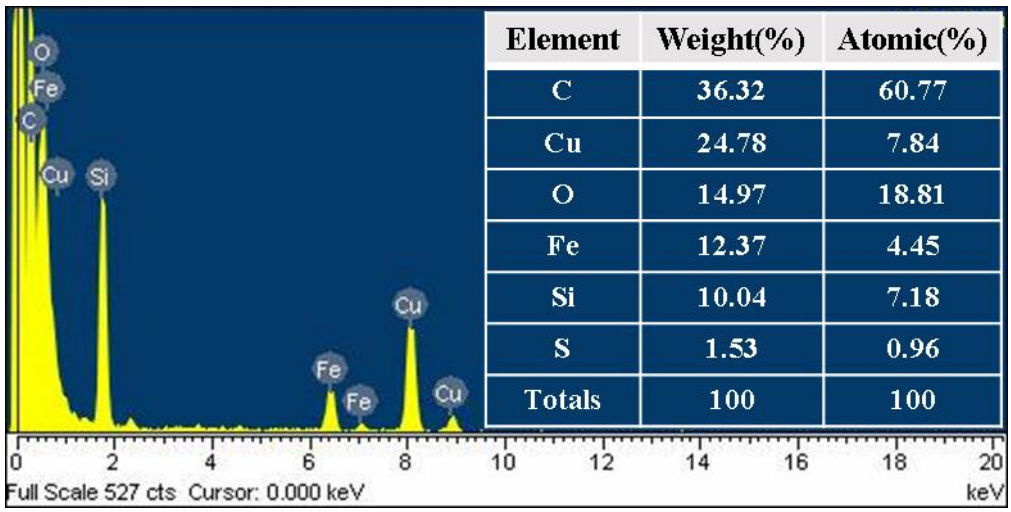

Element	Weight(%)	Atomic(%)
C	36.32	60.77
Cu	24.78	7.84
O	14.97	18.81
Fe	12.37	4.45
Si	10.04	7.18
S	1.53	0.96
Totals	100	100

Figure 3. EDS analysis of the synthesized FHA NPs

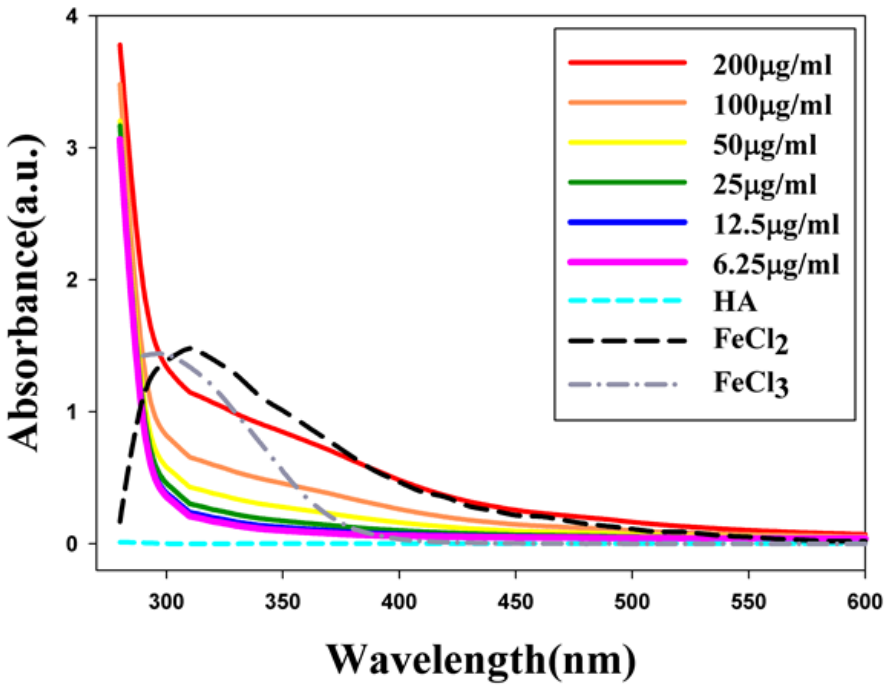

Figure 4. UV-visible spectrum comparison of HA in DW, $FeCl_2$, $FeCl_3$ as Synthetic materials and FHA NPs by concentration. The absorbance spectrum of different concentrations of FHA NPs was measured by UV-visible spectrophotometer. Each FHA NPs concentration was measured triplicates.

The particle size and shapes were confirmed by the SEM and TEM image (Figure2d). The energy dispersive X-ray spectrometry (EDS) of FHA NPs was shown in Figure 3. The peak of other such as Cu and Si except for Fe on the spectra originates from TEM grid.

The actual amount of internalized Fe in FHA NPs was determined by ICP-AES to quantify the amount of Fe as a function of concentration of FHA NPs for the subsequent *in vitro* assay (Figure 2e). As the concentration of FHA NPs increased, the loading efficiency increased linearly with increasing iron ion concentration (R^2=0.9971). Zeta potential measurements show 30±1.9mV in pH 4, compared to a 16±0.7mV in pH 7 and −8±1.2mV in pH 10, due to the acidity of the carboxyl groups. The average results of Zeta potential were reasonably narrow distributions at pH 4 and largely positive. According to pH-triggered size change, zeta potential values strongly depend on the pH. We have monitored the average value and dispersity of size. Thus, we monitored the size and PDI for 6 months by detecting the mean and variance. The stability of FHA NPs in storage condition (DW with 0.005 M HCl) were maintained as the size (105±2 nm) and PDI (0.24±0.01) for 6 months that show the excellent physicochemical stability (Figure 2f).

The size of FHA NPs at pH 4 were measured about 400 nm that

was agglomerated than in pH 7 and size in pH 10 shows 150 nm that was loosened HA polymer (**Figure 2g**). **Figure 2h** is a photograph image to confirm the difference between the storage state in DW (**i**) and in 0.005M HCl (**ii**). It can be confirmed that the image is well dispersed with the property of HA with COO^- functional group to the negative charge. And we confirmed FHA NPs formation by different absorbance of UV-Vis spectrum between HA NPs including Fe, and control groups (HA only, $FeCl_2$ only, and $FeCl_3$ only) **(Figure 4)**.

We constructed FHA NPs through a natural secondary bond, thereby forming a pre-gel solution of Fe^{2+}/Fe^{3+}-hyaluronic acid. These secondary bonding of COOH of hyaluronic acid of Fe^{2+} and Fe^{3+} can be explained based on the automatic crosslinking mechanism.[25, 26] Due to the nature of secondary bonding, the individual adhesive force may not be stronger than anthropogenic chemical bonds. But, as the particles aggregate, the total interfacial surface area increases, which can result in the total bonding strength may be improved.

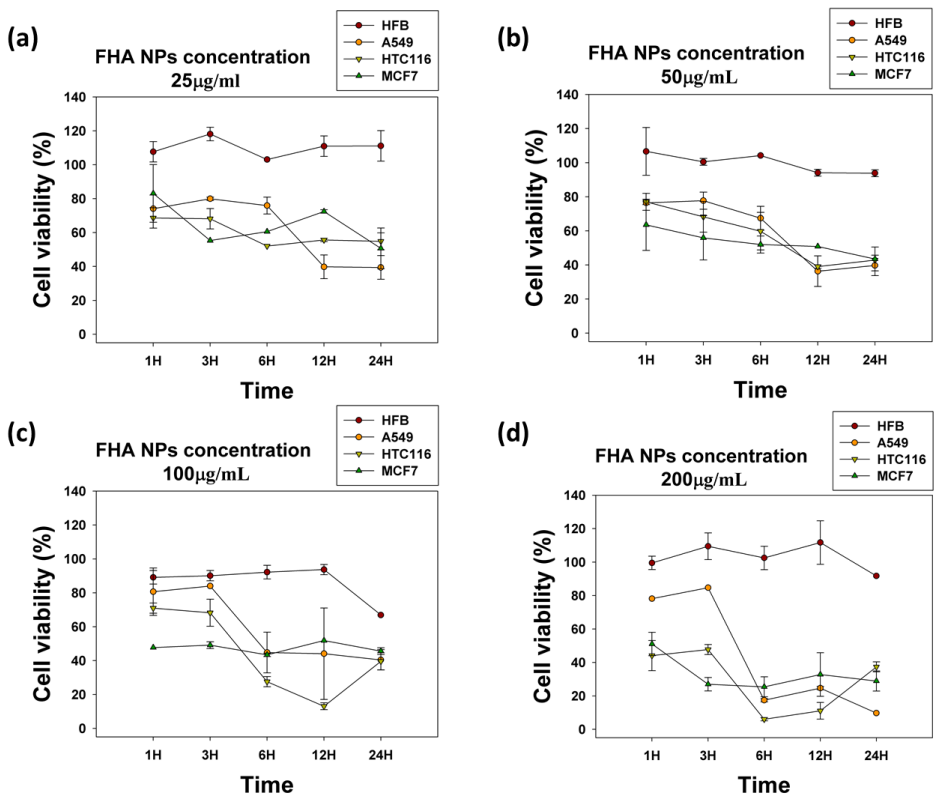

Figure 5. Determination of cell viability over time according to the concentration of FHA NP by measuring CCK-8 assay (a) Cell viability at FHA NP concentration of 25 μg/mL by time. (b) Cell viability at FHA NP concentration of 50 μg/mL by time. (c) Cell viability at FHA NP concentration of 100 μg/mL by time. (d) Cell viability at FHA NP concentration of 200 μg/mL by time.

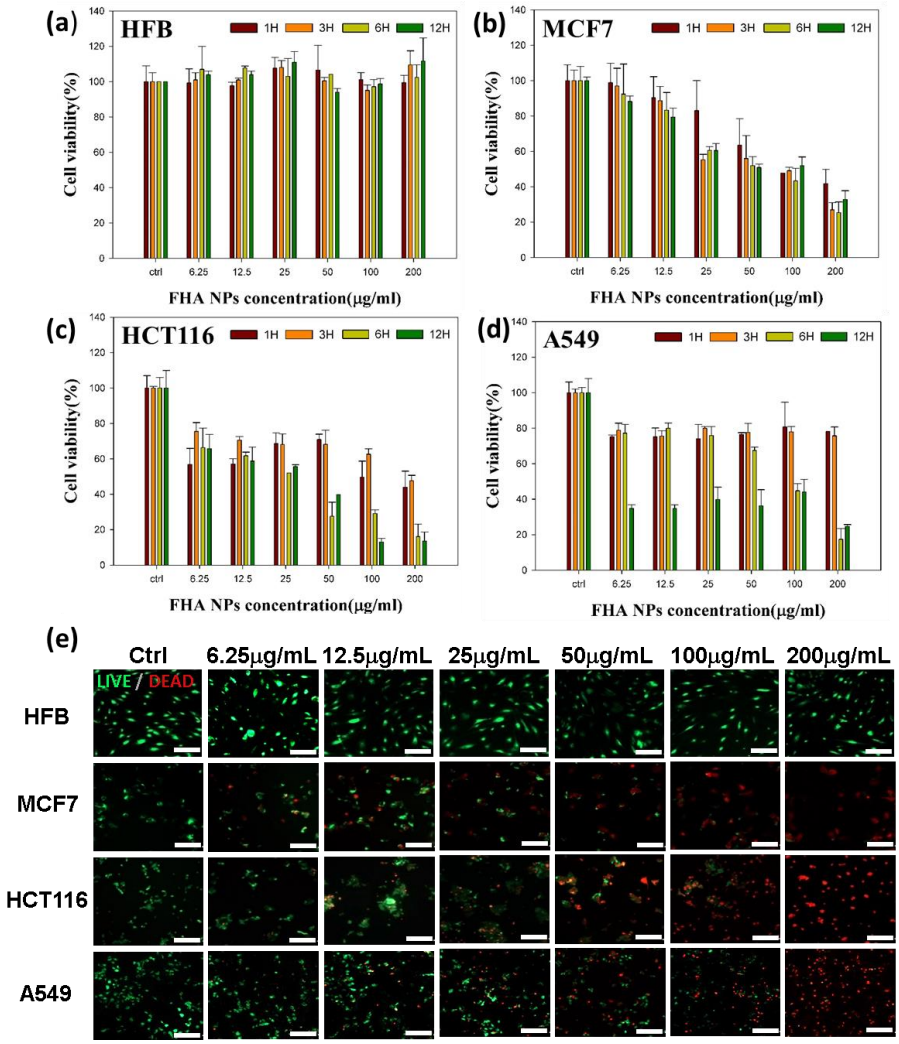

Figure 6. Comparison of the viability induced by HANP. (a)HFB, (b), MCF7, (c)HCT116, (d)A549, Cytotoxic effects of different concentration of FHA NPs, as measured by a Cell Counting Kit-8 assay. (e) Images of live-dead assay 1h, 3h, 6h, 12h after those were treated with different concentration of FHA NPs (scale bar: 100 μm)

To confirm the cell viability, we treated various concentrations of FHA NPs ranging from 6.25 μg/mL to 200 μg/mL for 1, 3, 6, and 12 hours to cancer cell lines, and analyzed Cell Counting Kit-8 (CCK-8) assay (**Figure 5**). Except for MCF7 cells, cell death was observed significantly induced than normal cell Human fibroblast cells (HFB) at a low concentration of 6.25 μg/mL of FHA NPs. In **Figure 6a, 6b, 6c, 6d,** the viability of HFB and human breast adenocarcinoma cells (MCF7), human colon carcinoma cells (HCT116) and human lung carcinoma cells (A549) cells were compared. At the concentration of 200 μg/mL of FHA NPs, compared with the FHA NPs-free control, MCF7, HCT116, and A549 cells were survived only 32.7±5%, 13.7±5%, and 23.6±1% after 12 hours, respectively. In other words, the viability of cancer cells at 1, 3, 6, and 12 hours was significantly lower than normal cells. In normal cells, increasing the concentration of FHA NPs and long uptaken time did not affect cell survival. From these results, we found that FHA NPs were successfully induced cancer cell death without affecting normal cells. Although the cell death rate and the concentration of the affected FHA NPs were different depending on the characteristics of each cancer cell, the tendency of the cells to die by the influence of the FHA NPs containing Fe in cancer cells was the same.

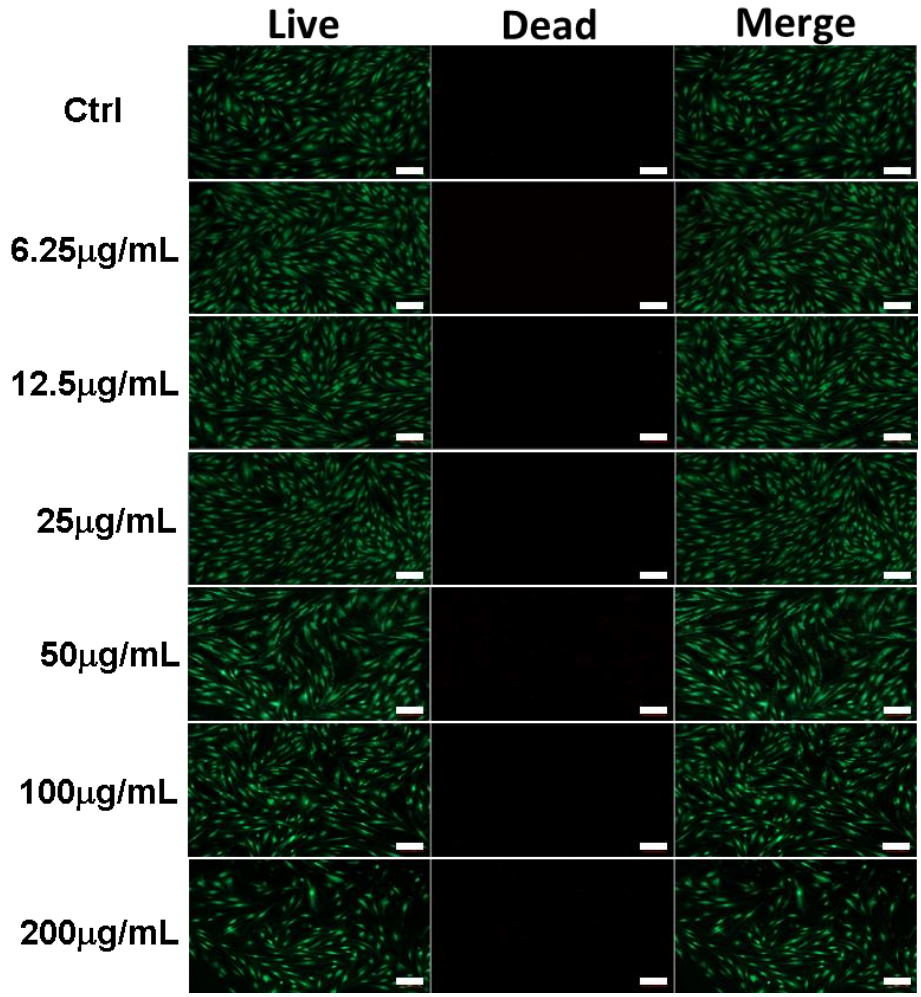

Figure 7. Images of live-dead assay incubated with HFB and different concentration of FHA NPs for12 hours. Scale bar indicates 100 μm. Live (green) and dead (red)

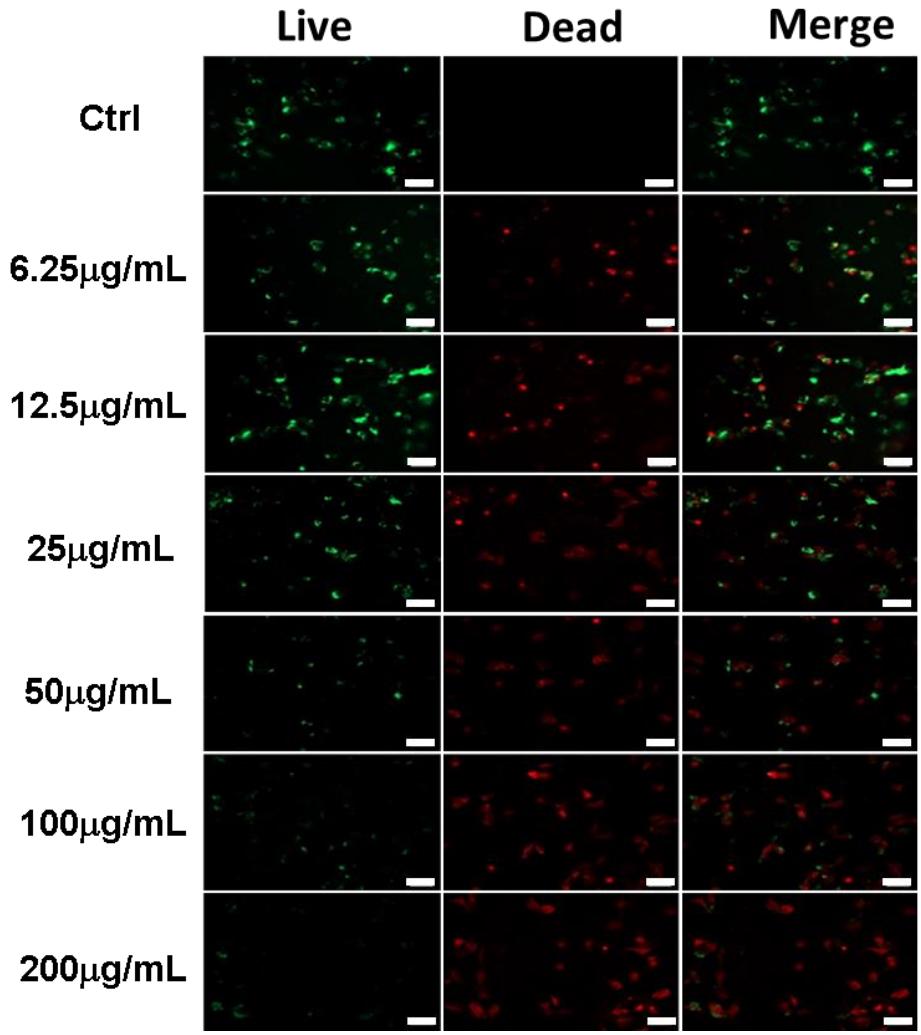

Figure 8. Images of live-dead assay incubated with MCF7 and different concentration of FHA NPs for12 hours. Scale bar indicates 100 μm. Live (green) and dead (red)

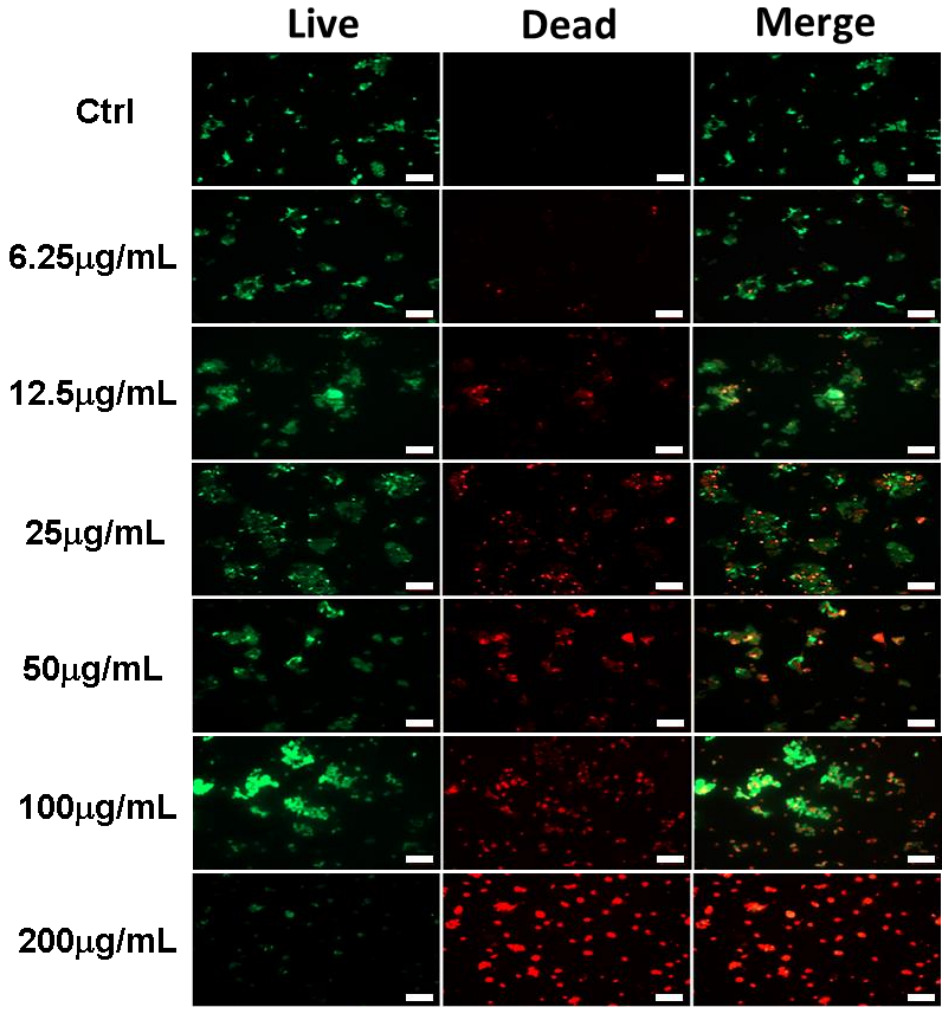

Figure 9. Images of live-dead assay incubated with HCT116 and different concentration of FHA NPs for12 hours. Scale bar indicates 100 μm. Live (green) and dead (red)

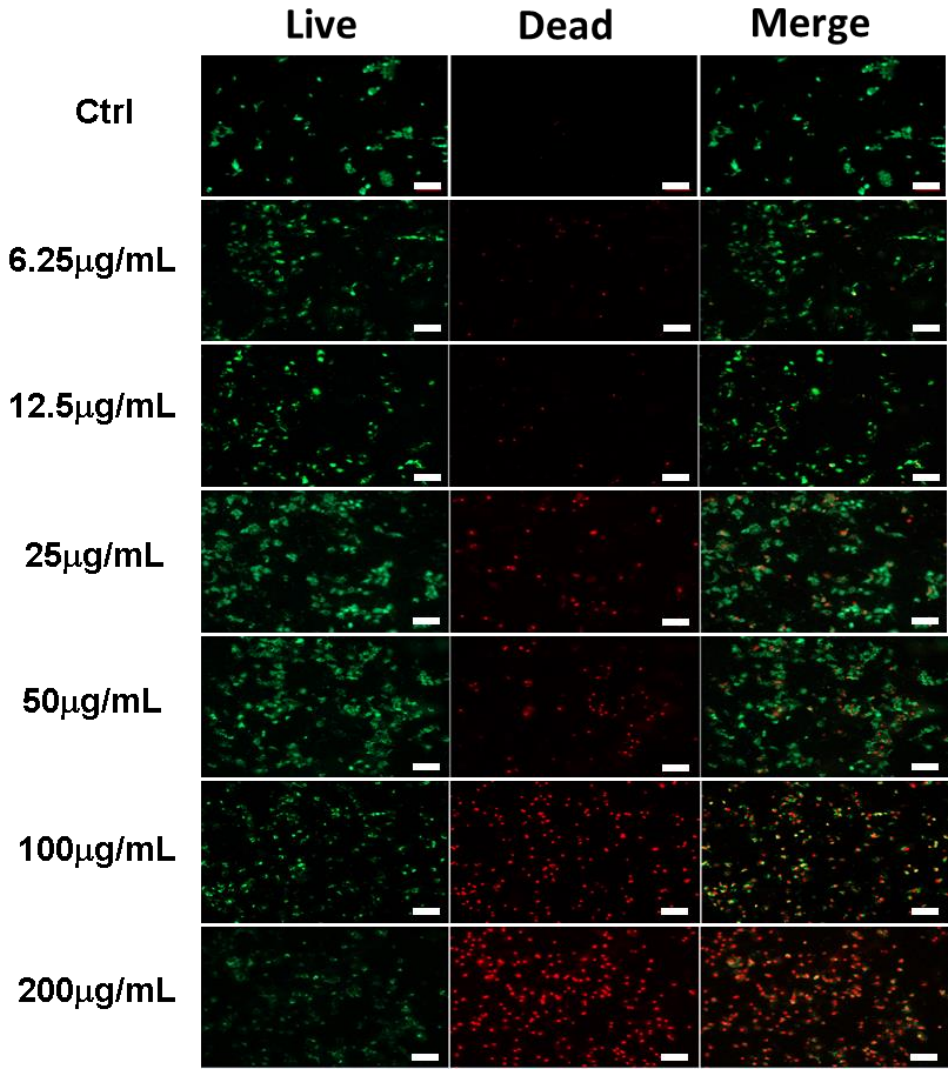

Figure 10. Images of live-dead assay incubated with A549 and different concentration of FHA NPs for12 hours. Scale bar indicates 100 μm. Live (green) and dead (red)

To study the cytotoxicity and biocompatibility of nanoparticles, live-dead images of normal cells (FHB) and cancer cells (MCF7, HCT116, A549) were obtained at 12 hours after treatment with different concentrations (6.25 μg/mL to 200 μg/mL) of FHA NPs (scale bar: 100μm) (**Figure 6e, Figure 7, 8, 9, 10**). Green and red color indicates live and dead cells, respectively. As the concentration of NP increases from 6.25 μg/mL to 20 μg/mL, the living cells decreased and the dead cells increased. These results show that cell death increases as the concentration of FHA NPs increased, which was the same as the tendency of viability confirmed by CCK-8.

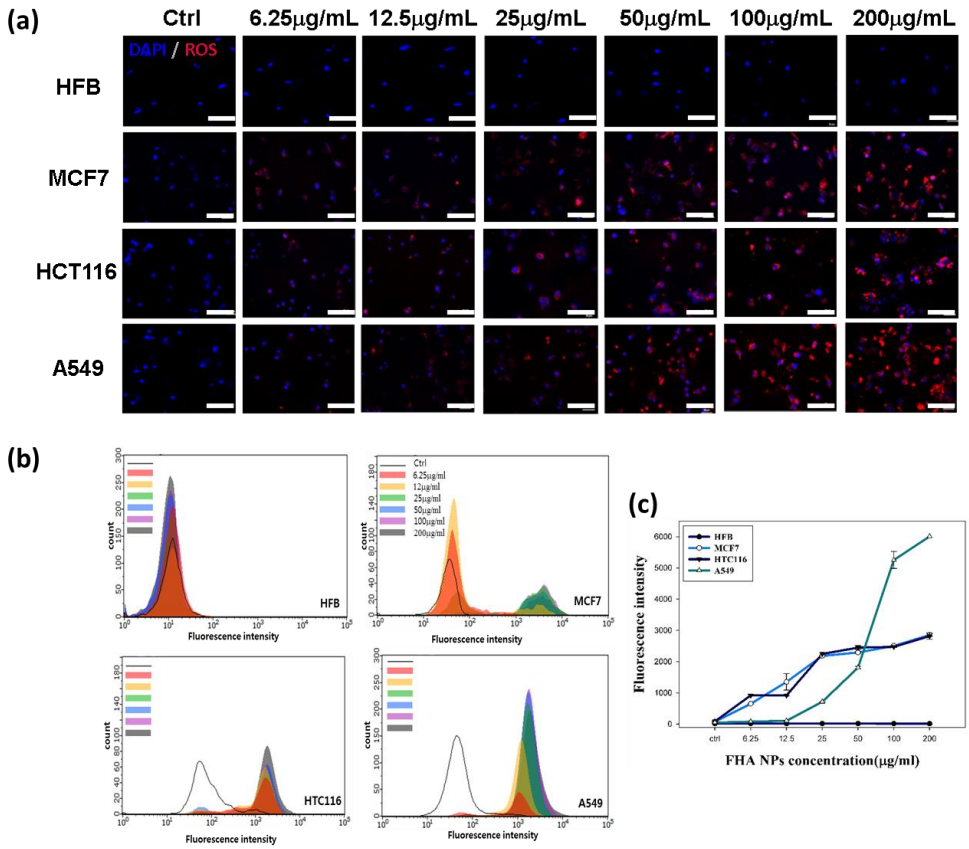

Figure 11. Confocal microscope analysis of intracellular ROS generation. (a) Fluorescent images of CellROX Orange representing ROS production. The scale bar is 50μm. (blue and red color indicates nuclear, and ROS expression, respectively) (b) FACS analysis for ROS quantification. FACS analysis was performed at 12 hours after treatment. Data represent three independent experiments. (c) Quantification of fluorescence intensity of ROS according to NP concentration using FAC for each cell line

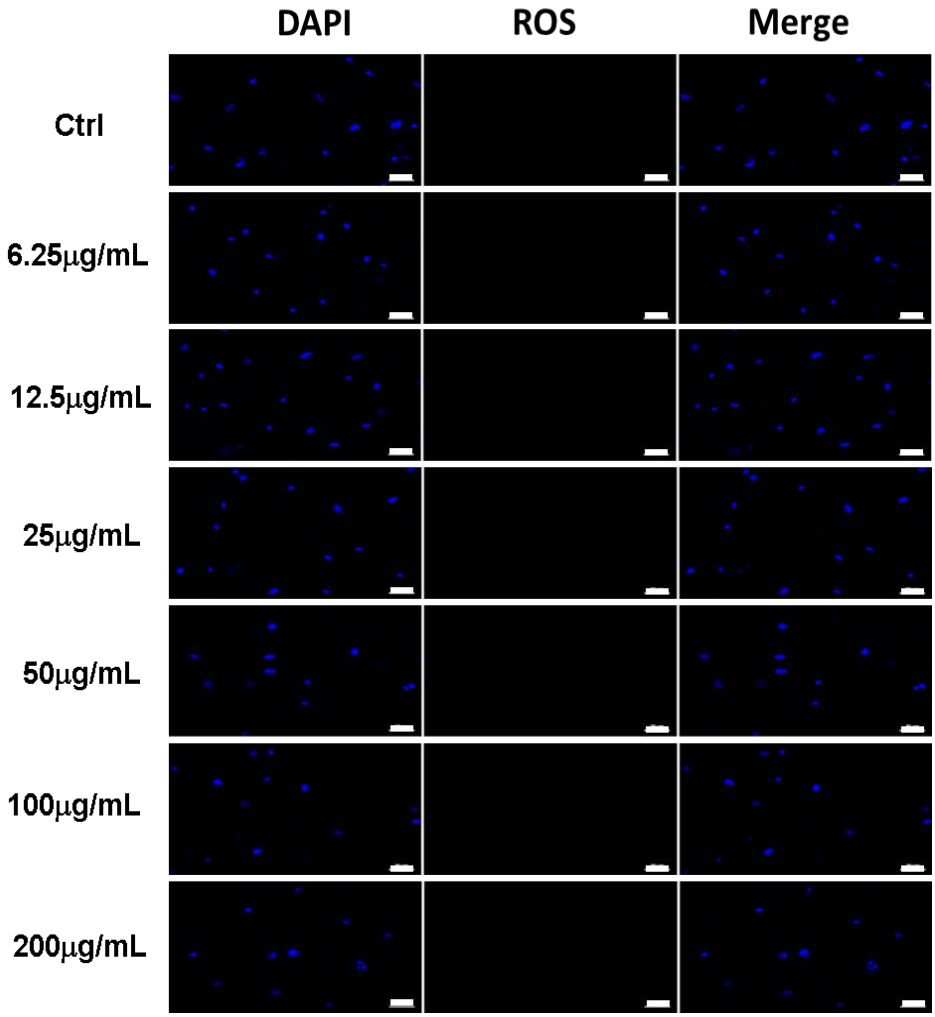

Figure 12. Confocal microscope analysis of intracellular ROS generation incubated with HFB and different concentration of FHA NPs for12 hours. Nucleus (blue) and ROS (red), Scale bar : 50μm

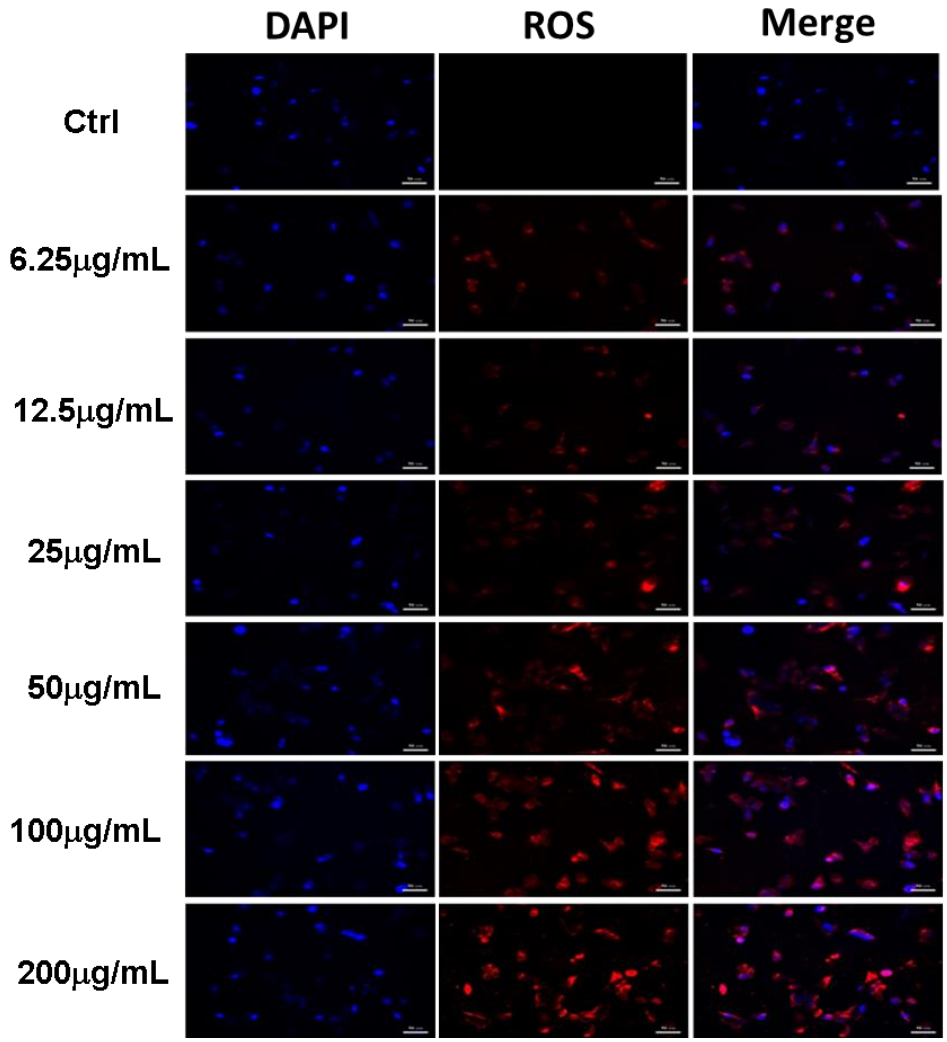

Figure 13. Confocal microscope analysis of intracellular ROS generation incubated with MCF7 and different concentration of FHA NPs for12 hours. Nucleus (blue) and ROS (red), Scale bar : 50μm

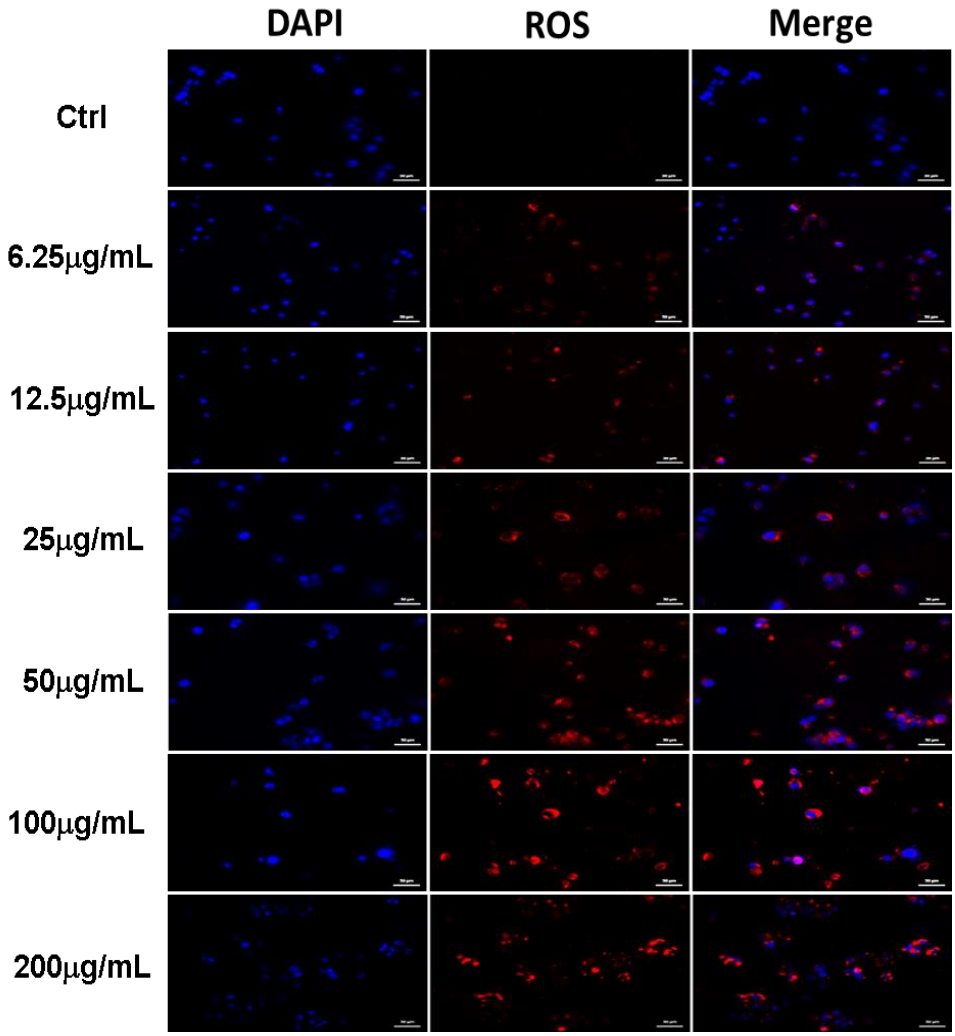

Figure 14. Confocal microscope analysis of intracellular ROS generation incubated with HCT116 and different concentration of FHA NPs for12 hours. Nucleus (blue) and ROS (red), Scale bar : 50μm

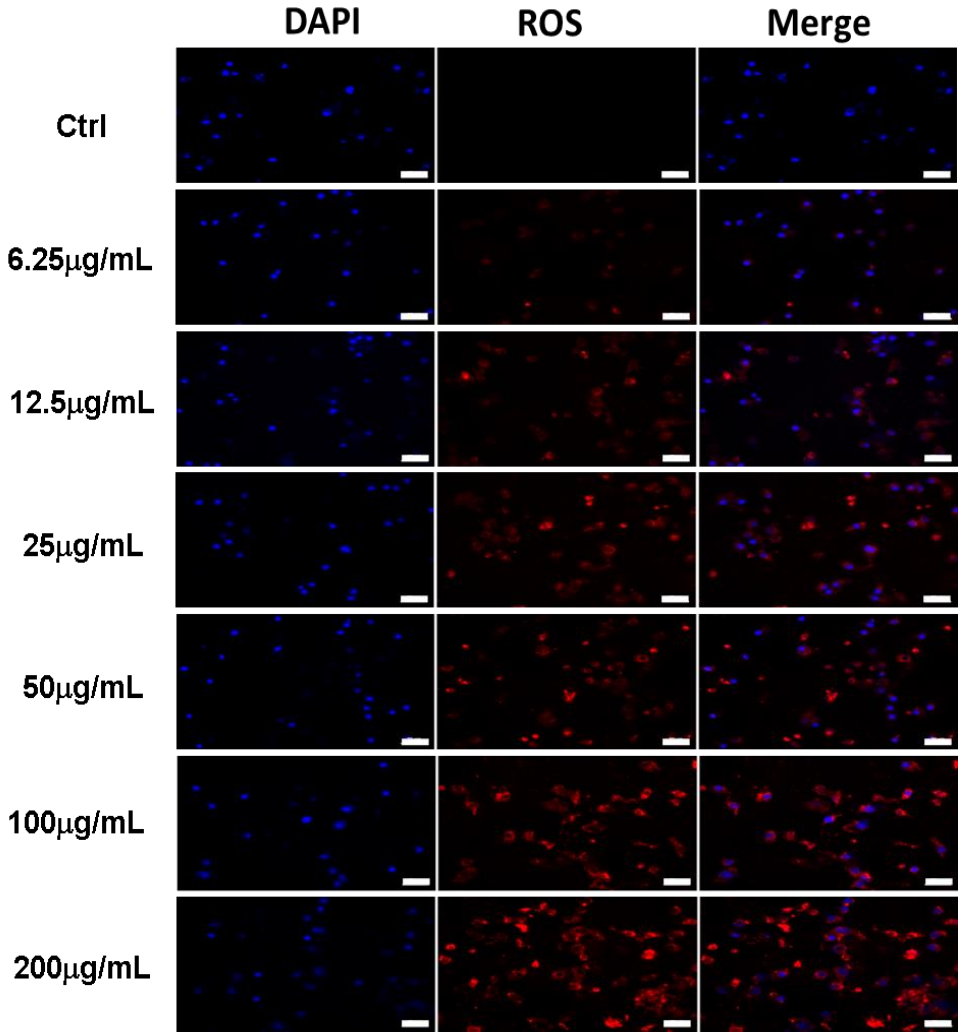

Figure 15. Confocal microscope analysis of intracellular ROS generation incubated with A549 and different concentration of FHA NPs for12 hours. Nucleus (blue) and ROS (red), Scale bar : 50μm

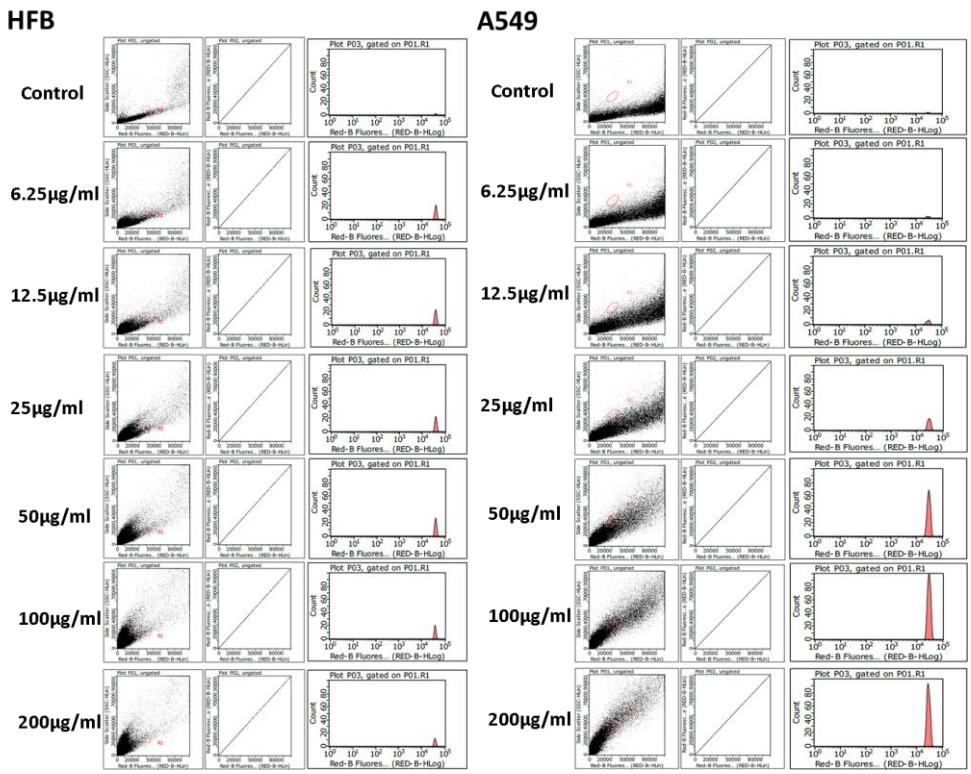

Figure 16. FACS analysis of increased ROS expression in HFB, A549 by FHA NP concentration.

We observed the expression of ROS, a key component of accumulation by the Fenton reaction in the molecular mechanisms of ferroptosis. In **Figure 11a**, the presence of ROS at different FHA NPs concentrations was confirmed by confocal microscopy. (Scale bar: 50μm) (**Figure 12, 13, 14, 15**) As the concentration increased, the expression of ROS, a key factor of ferroptosis, was detected. We quantified ROS expression by flow cytometry cell sortings (FACS). In HFB, ROS expression was not show the fluorescence intensity with increasing FHA NPs concentration, however, fluorescence intensity was increased with increasing NP concentration in MCF7, HCT116 and A549 (**Figure 11b, Figure 16**). And, in **Figure 11c**, fluorescence intensities of ROS were quantified according to FHA NPs concentration using FAC for each cell line. Thus, we confirmed that FHA NPs is cancer cell-specific targeting NPs by ferroptosis.

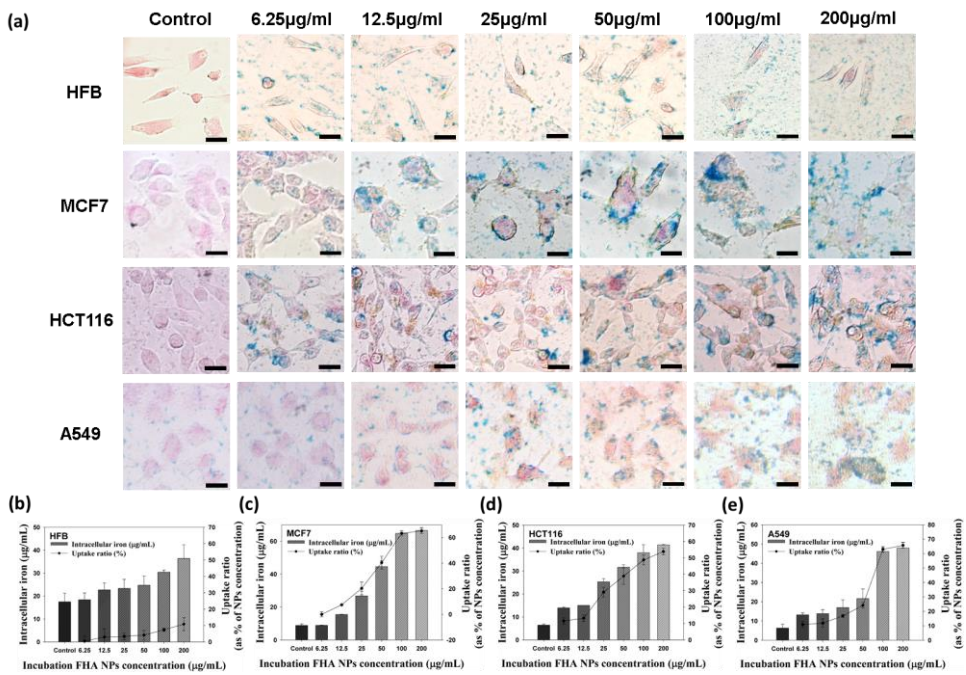

Figure 17. Prussian blue staining and ICP-AES quantification of intracellular Fe contents. (a) Microscopic images of Prussian blue staining MCF7, HTC116, A549, and HFB incubated with HFA NPs at different concentration, followed by the counterstain nuclear fast red. Light pink coloring of cytoplasm, dark pink coloring of nuclei and blue coloring of the Fe core of the molecules were seen. The scale bar is 20 μm (b) HFB (c) MCF7 (d) HCT116 (e) A549, Quantification of internalized NPs in cells by ICP-AES and uptake ratio concentration.

Quantitative assessment of cellular uptake of FHA NP is essential to confirm the absorbed amount of Fe in cells. Prussian blue assay is widely used to measure the cellular Fe content, relying on formed after reaction of Fe ion in a cell. To evaluate quantitative cellular uptake of FHA NPs, we stained cells with Prussian blue at different concentration of FHA NP (Figure 17a). In HFB normal cells, the tendency of accumulation by Fe ions could not be confirmed through the particle accumulation increased on the cell surface. However, we observed the amount of Fe accumulated inside the cell increases as the concentration increases in cancer cells. Figures 17b~17e shows that quantification of the intracellular Fe concentration by ICP-AES, and these results indicate cellular uptake ratio of FHA NPs. The amounts of Fe contained in each cell were different from each other, and the amount of endocytosis was also different with same concentration of NPs. In comparison with normal cells and cancer cells, cancer cells are considered inducing Fe accumulation by continuous chain reaction due to large amount of Fe in the cells than HFB.

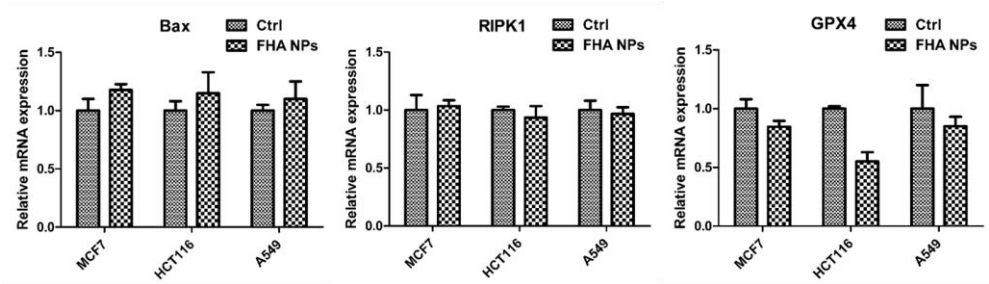

Figure 18. mRNA expression confirmation through real time RT-PCR. The expression level was calculated using the actin gene as an internal standard and the $\triangle\triangle C_T$ method was used for relative quantification.

We have performed real time RT-PCR to confirm the expression of ROS and cell death by ferroptosis (**Figure 18**). Bax, a key determinant of apoptosis expression, RIPK1, which confirms the development of Necrosis, and GPX4, a key factor known as a negative regulator of ferroptosis were used. GPX 4 is a substance that converts reduced GSH to oxidized glutathione (GSSG) while reducing lipid peroxide to the corresponding alcohol or free hydrogen peroxide, and GPX4 is also reported that overexpression induces resistance to RSL3. Other research groups have reported that GPX4 knockdown induces cell death, a key component of the negative regulator of ferroptosis.[29] In comparison between relative mRNA expression, there was no significant difference between Bax and RIPK1 in MCF7, HCT116, and A549. However, GPX4 was significantly decreased compared to the control group which did not treat FHA NPs. In addition, ferroptosis proceeded by reduction of GPX4 with FHA NPs, unlike control group. Expression of Bax was slightly expressed than in RIPK, that is, ferroptosis was more affected in apoptosis than necrosis.[18] From these results, we suggest FHA NPs is a promising platform to induce the cancer therapy by ferroptosis, but, the further studies on the relationship between ferroptosis and apoptosis will be needed.

Although the molecular mechanism of ferroptosis has not been

fully elucidated, a number of drugs are known to induce and inhibit ferroptosis. Ferrostain-1 and α-tocopherol, known as vitamin E, are a negative regulator of ferroptosis by inhibiting lipid peroxidation. Ferrostain-1 inhibits ROS accumulation by lipid oxidation, and inhibits antioxidant effect by vitamine E.[30] RSL3 binds to GPX4 and then inactivates GPX4 to allow the iron-dependent accumulation of ROS from lipid peroxidation, resulting in ferroptosis by inhibition of downstream regulators.[29] Thus, three drugs including RSL3, Ferrostatin-1, and α-Tocopherol (vitamin E) were used to confirm the ferroptotic activity and inhibitory effect which inhibit lipid peroxidation by ROS.

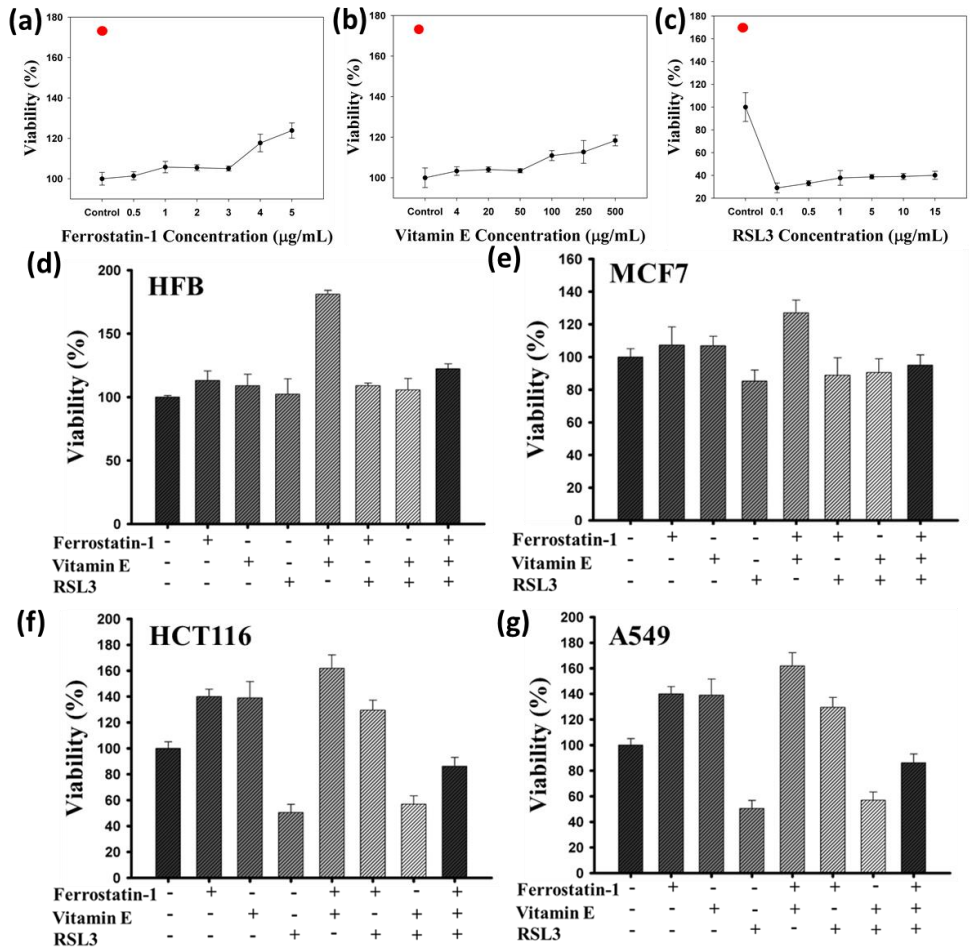

Figure 19. Confirmation of lipid peroxidation inhibitory effect using Ferrostatin-1, Vitamin. E, RSL3. A Confirmation of effects at each concentration for drug concentration selection (a)Ferrostatin-1, (b) Vitamin E, (c) RSL3. (d) HFB (e) MCF7 (f) HCT116 (g) A549, Confirmation of lipid peroxidation inhibitory effect. Ferrostatin-1and Vitamin E inhibits lipid peroxidation and cell death, while RSL3 induces ROS accumulation, lipid peroxidation, and cell death

First, A549 cells were treated at a concentration of 200 μg/mL for 12 hours according to the concentration of each drug. (**Figure 19a, 19b, 19c**) The red dot on the upper left is the viability that shows without FHA NPs, and more than 70% of cell death was observed after treat FHA NPs. Appropriate drug concentration was selected from preliminary experiments, the concentrations used at 4 μg/mL for ferrostain-1, 100 μg/mL for vitamin E, and 1 μg/mL for RSL3. (**Figure 19d~19g**) Ferrostatin-1 and vitamin E increased viability by inhibiting lipid peroxidation and decreased RSL3 activity by treatment with a single drug, respectively. The viability of the drug was confirmed by complementation and offsetting with both drugs. The effects of drugs on HFB were not significantly different, but, the activity and inhibitory of MCF7, HCT116, and A549 cells was confirmed. In other words, the effects of drugs were found to be fast and significant with A549 cells. However, the biologic properties of each cell are different, and it is necessary to study the ferroptosis-based therapeutic drug according to the type of cancer.

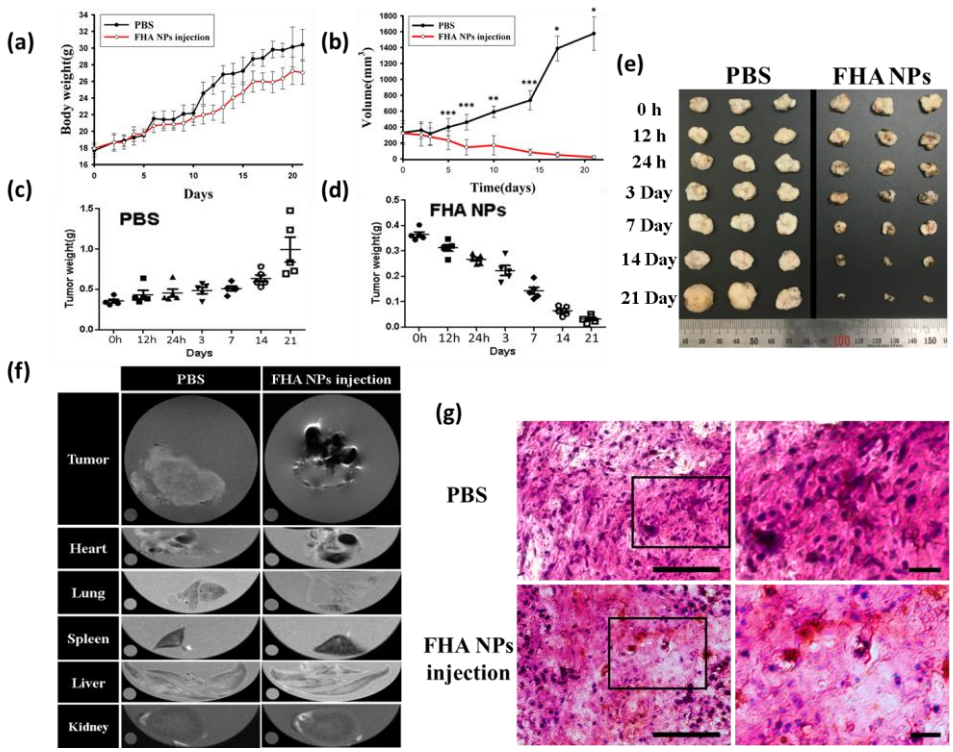

Figure 20. Identification by *in vivo*. (a) Profiling body weight change in tumor-bearing athymic nude mice. (b) Differences in tumor volume after injecting the PBS and FHA NPs. (c)(d) The time-dependent graph of tumor weight after injecting the PBS and FHA NPs. (e) Images of tumor suppression by cancer cell death. (f) Confirmation of Fe accumulation in organs and tumor by MRI at control and FHA NPs injected group. (g) Images of H & E staining with tumor region. The scale bar is 50 μm

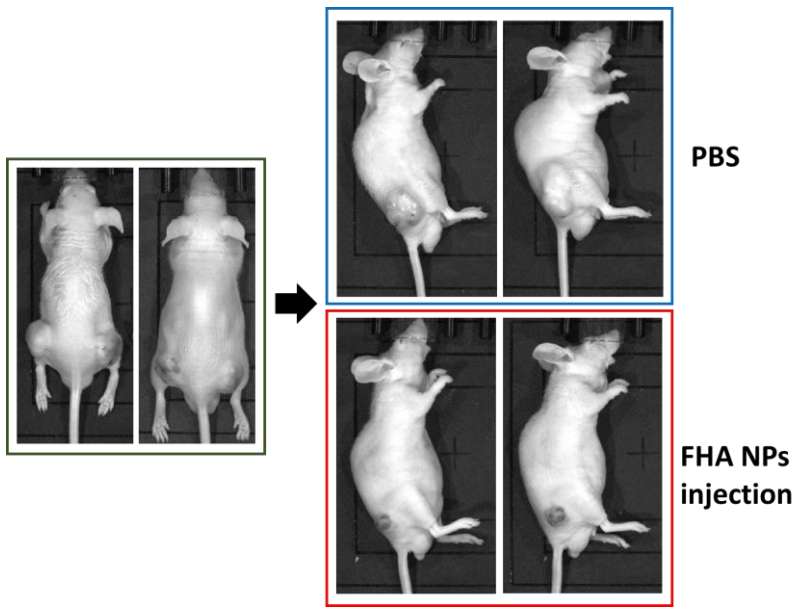

Figure 21. IVIS 200 optical image of tumor size changes in PBS-injected group and FHA NPs treated group after 21 days. The upper image shows when PBS was injected and the lower image shows when FHA NPs were injected

For *in vivo* test, A549 cells were subcutaneously injected in the mice. FHA NPs were injected at a peritumoral region with a concentration of 8 mg/kg every 24 hours. Groups were divided into groups of 0, 12, 24 hours and 3, 7, 14, 21 days and profiled daily weight changes (**Figure 20a**). The volume of tumor injected with FHA NPs was significantly reduced, while the control was increased t with the passage of time. After 21 days of xenograft formation, the 330 mm^3 tumor volume was reduced to 32 ± 12 mm^3, leaving only about 10% of the tumor remained, and the control group with PBS had grown to 1500 after 21 days (**Figure 20b**). **Figure 21** is IVIS 200 optical image of tumor size changes in PBS-injected group and FHA NPs treated group after 21 days.

The weight of the tumor increased from 0.35g to 1.4 g in the PBS-injected group, the tumor weight was decreased from 0.35g to 0.03 g in the FHA NPs injected group. (**Figure 20c, 20d**) **Figure 20e** show a photograph of tumor suppression by cell death. The effect of FHA NPs was confirmed by MRI in the organ. Compared with the control group, FHA NPs injected groups were showed no difference in heart, lung, spleen, liver, and kidney, thus, we confirmed that Fe accumulation was concentrated only in the tumor. (**Figure 20f**) **Figure 20g** shows the results of H & E staining in control and experimental group. The right enlarged image shown by the arrow

was shown that nuclei were uniformly distributed in the tumor injected with PBS due to the without cell death, but FHA NPs injected group was observed few nuclei by cell death. Thus, we confirmed that ferroptotic cell death by FHA NPs *in vivo* and confirmed the possibility of various studies using this system.

Chapter 4. Conclusion

In summary, we used a molecular mechanism of iron-dependent ferroptosis by preparing the biocompatible HA NPs including Fe ion in this study. Based on the specific targeting of CD44 as HA receptor, which is particularly expressed in cancer cells, we made tumor-targeted FHA NPs that size is a 100 nm, and we confirmed the possibility of scaling up due to the easy manufacturing method. We found that FHA NPs induced ROS expression *in vitro* by the effect of Fe reaction, and showed about 80% cell death after cellular uptake for 12 hours. In addition, the initial size of xenotransplant tumors was measured 330mm^3, but tumor decreased to 30 mm^3 (about 90% of tumor) after 21 days. In other words, this smart nanoparticle, composed of only harmless components, is ideal to apply for cancer therapy by inducing the ferroptosis. We have confirmed the induction of ferroptosis by FHA NPs, and we suggest many directions and possibilities expand it in this study. This new nanoparticle platform is expected to be one of the effective tools for cancer therapy.

References

[1] K. Riehemann, S.W. Schneider, T.A. Luger, B. Godin, M. Ferrari, H. Fuchs, Nanomedicine—Challenge and Perspectives, Angew Chem Int Edit 48(5) (2009) 872-897.

[2] A. Shapira, Y.D. Livney, H.J. Broxterman, Y.G. Assaraf, Nanomedicine for targeted cancer therapy: Towards the overcoming of drug resistance, Drug Resist Update 14(3) (2011) 150-163.

[3] A. Wicki, D. Witzigmann, V. Balasubramanian, J. Huwyler, Nanomedicine in cancer therapy: Challenges, opportunities, and clinical applications, J Control Release 200 (2015) 138-157.

[4] J.J. Shi, P.W. Kantoff, R. Wooster, O.C. Farokhzad, Cancer nanomedicine: progress, challenges and opportunities, Nat Rev Cancer 17(1) (2017) 20-37.

[5] D.E. Owens, N.A. Peppas, Opsonization, biodistribution, and pharmacokinetics of polymeric nanoparticles, Int J Pharm 307(1) (2006) 93-102.

[6] J.A. Champion, Y.K. Katare, S. Mitragotri, Particle shape: A new design parameter for micro- and nanoscale drug delivery carriers, J Control Release 121(1-2) (2007) 3-9.

[7] G.H. Heppner, Tumor Heterogeneity, Cancer Res 44(6) (1984) 2259-2265.

[8] B. Sumer, J.M. Gao, Theranostic nanomedicine for cancer, Nanomedicine-Uk 3(2) (2008) 137-140.

[9] A.Z. Wilczewska, K. Niemirowicz, K.H. Markiewicz, H. Car, Nanoparticles as drug delivery systems, Pharmacol Rep 64(5) (2012) 1020-1037.

[10] R. Foldbjerg, P. Olesen, M. Hougaard, D.A. Dang, H.J.

Hoffmann, H. Autrup, PVP-coated silver nanoparticles and silver ions induce reactive oxygen species, apoptosis and necrosis in THP-1 monocytes, Toxicol Lett 190(2) (2009) 156-162.
[11] A. Ito, H. Honda, T. Kobayashi, Cancer immunotherapy based on intracellular hyperthermia using magnetite nanoparticles: a novel concept of "heat-controlled necrosis" with heat shock protein expression, Cancer Immunol Immun 55(3) (2006) 320-328.
[12] Y. Pan, A. Leifert, D. Ruau, S. Neuss, J. Bornemann, G. Schmid, W. Brandau, U. Simon, W. Jahnen-Dechent, Gold nanoparticles of diameter 1.4 nm trigger necrosis by oxidative stress and mitochondrial damage, Small 5(18) (2009) 2067-76.
[13] M. Premanathan, K. Karthikeyan, K. Jeyasubramanian, G. Manivannan, Selective toxicity of ZnO nanoparticles toward Gram-positive bacteria and cancer cells by apoptosis through lipid peroxidation, Nanomed-Nanotechnol 7(2) (2011) 184-192.
[14] R.G. Stevens, D.Y. Jones, M.S. Micozzi, P.R. Taylor, Body Iron Stores and the Risk of Cancer, New Engl J Med 319(16) (1988) 1047-1052.
[15] R.L. Nelson, Iron and colorectal cancer risk: Human studies, Nutr Rev 59(5) (2001) 140-148.
[16] D.A. Pratt, K.A. Tallman, N.A. Porter, Free Radical Oxidation of Polyunsaturated Lipids: New Mechanistic Insights and the Development of Peroxyl Radical Clocks, Accounts Chem Res 44(6) (2011) 458-467.
[17] S.E. Kim, L. Zhang, K. Ma, M. Riegman, F. Chen, I. Ingold, M. Conrad, M.Z. Turker, M.H. Gao, X.J. Jiang, S. Monette, M. Pauliah, M. Gonen, P. Zanzonico, T. Quinn, U. Wiesner, M.S. Bradbury, M. Overholtzer, Ultrasmall nanoparticles induce ferroptosis in nutrient-deprived cancer cells and suppress tumour growth, Nat

Nanotechnol 11(11) (2016) 977-985.
[18] D.W. Zheng, Q. Lei, J.Y. Zhu, J.X. Fan, C.X. Li, C. Li, Z.S. Xu, S.X. Cheng, X.Z. Zhang, Switching Apoptosis to Ferroptosis: Metal-Organic Network for High-Efficiency Anticancer Therapy, Nano Lett 17(1) (2017) 284-291.
[19] R.J. Peach, D. Hollenbaugh, I. Stamenkovic, A. Aruffo, Identification of Hyaluronic-Acid Binding-Sites in the Extracellular Domain of Cd44, J Cell Biol 122(1) (1993) 257-264.
[20] J. Lesley, Q. He, K. Miyake, A. Hamann, R. Hyman, P.W. Kincade, Requirements for Hyaluronic-Acid Binding by Cd44 - a Role for the Cytoplasmic Domain and Activation by Antibody, J Exp Med 175(1) (1992) 257-266.
[21] Y. Luo, G.D. Prestwich, Synthesis and selective cytotoxicity of a hyaluronic acid-antitumor bioconjugate, Bioconjugate Chem 10(5) (1999) 755-763.
[22] M. Zoller, CD44: can a cancer-initiating cell profit from an abundantly expressed molecule?, Nat Rev Cancer 11(4) (2011) 254-267.
[23] W.T. Winter, S. Arnott, Hyaluronic acid: the role of divalent cations in conformation and packing, J Mol Biol 117(3) (1977) 761-84.
[24] H. Shagholani, S.M. Ghoreishi, M. Mousazadeh, Improvement of interaction between PVA and chitosan via magnetite nanoparticles for drug delivery application, Int J Biol Macromol 78 (2015) 130-136.
[25] A. Okamoto, Miyoshi, Teruzoh, A Biocompatible gel of Hyaluronan, Hyaluronan 1 (2002) 285-282.
[26] M.N. Collins, C. Birkinshaw, Physical properties of crosslinked hyaluronic acid hydrogels, J Mater Sci-Mater M 19(11) (2008)

3335-3343.

[27] L. Jiang, N. Kon, T.Y. Li, S.J. Wang, T. Su, H. Hibshoosh, R. Baer, W. Gu, Ferroptosis as a p53-mediated activity during tumour suppression, Nature 520(7545) (2015) 57-+.

[28] M.H. Gao, P. Monian, Q.H. Pan, W. Zhang, J. Xiang, X.J. Jiang, Ferroptosis is an autophagic cell death process, Cell Res 26(9) (2016) 1021-1032.

[29] W.S. Yang, R. SriRamaratnam, M.E. Welsch, K. Shimada, R. Skouta, V.S. Viswanathan, J.H. Cheah, P.A. Clemons, A.F. Shamji, C.B. Clish, L.M. Brown, A.W. Girotti, V.W. Cornish, S.L. Schreiber, B.R. Stockwell, Regulation of Ferroptotic Cancer Cell Death by GPX4, Cell 156(1-2) (2014) 317-331.

[30] S.J. Dixon, K.M. Lemberg, M.R. Lamprecht, R. Skouta, E.M. Zaitsev, C.E. Gleason, D.N. Patel, A.J. Bauer, A.M. Cantley, W.S. Yang, B. Morrison, B.R. Stockwell, Ferroptosis: An Iron-Dependent Form of Nonapoptotic Cell Death, Cell 149(5) (2012) 1060-1072.

국문초록

산화철을 함유한 히알루론산 나노입자를 이용한 페롭토시스 암세포사멸 조절에 관한 연구

배채원
나노융합전공
융합과학부
서울대학교 융합과학기술대학원

나노의학은 복잡하고 비균질적 특징을 가진 암을 극복하기 위한 새로운 치료 대안으로 떠오르고있다. 그 중에서 나노입자를 이용한 치료 잠재성이 지속적으로 밝혀지고 있으며, 부작용을 줄이고 정확하게 표적할 수 있는 연구가 활발히 진행되고 있다. 이러한 나노입자는 다양한 세포사멸 기전에 기초하여 연구되어 왔다. 본 연구에서는, 새로운 형태의 사멸 기전을 기반으로 나노입자를 제조하였고 이를 통한 암 치료 가능성을 제시한다.

페롭토시스(ferroptosis)는 생체내 필수 전이 금속인 철 (iron)이

세포사멸을 조절하는 중요한 역할을 하여 활성산소(ROS) 발생과 지질 과산화를 일으키는 것이다. 이는 기존에 알려진 자연 세포사멸이나 세포괴사와는 달리, 최근에 밝혀진 다른 형태의 세포사멸이다.

본 연구에서는, 페롭토시스를 일으키는 핵심 요소인 철과 생체 적합성 및 생분해성이 뛰어난 천연 고분자 히알루론산을 이용하여 물리 화학적 조절을 통해 암 표적 나노 입자를 제조하였다. 히알루론산은 암세포 표면에 특히 더 많이 발현되어 있는 CD44의 수용체를 가지고 있어 암세포 표적이 가능하다. 시험관 내 실험에서, 제조한 암 표적 나노입자를 12시간동안 200 μg/mL농도로 처리하였을 때 정상세포에는 영향 없이 약 80 %의 암세포가 선택적으로 사멸함을 확인하였고, 동물실험에서 330 mm^3의 종양이 21일 후 약 30 mm^3로 처음 대비 약 90 %가 줄어든 것을 관찰하였다.

결과적으로, 본 연구에서는 간편한 합성 방법으로 나노입자를 제조하여 암세포 사멸의 새로운 플랫폼을 제시하였다. 이는 나노의학 분야에서 응용할 수 있는 잠재력이 무한한 시스템으로서, 암 치료에 효과적인 대안이 될 것으로 기대한다.

주요어 : 페롭토시스, 암 나노의학, 철 기반 나노입자, 펜톤반응, 활성산소

학 번 : 2017-25383